Experimental Investigation of Oil Film Variation in Finite Line Contact Under Intermittent Motion

Haiping Li[1], Xinqing Wang[1], Haoyang Sun[2] and Jing Wang[1,*]

[1]*College of Mechanical Engineering, Donghua University, Shanghai, China*

[2]*College of Mechanical and Electrical Engineering, Qingdao University, Qingdao, China*

Abstract: The variation of oil film distribution in the line contact area of pin and disk was experimentally observed during a periodic intermittent motion. The study was conducted on a ball-disk optical interferometric test rig, with motion speed controlled by PLC programming. PAO40 oil was primarily used in the experiment, with the glass disk undergoing periodic motion of constant speed-deceleration-stop-acceleration, while the pin roller remained fixed. The results indicate that when the motion stops, a portion of the oil is entrapped in the center of the contact area. As the acceleration phase begins, this portion of the oil is gradually squeezed out of the contact area, and the oil film with lowest thickness at the entrance of the contact area moves towards the exit of the contact area, passing through the contact center. It can also be observed that during the entire process, an increase in speed increases the film thickness, while an increase in deceleration time, *i.e.*, a decrease in deceleration, reduces the film thickness during the stop phase.

Keywords: Intermittent Motion, Finite Line Contact, EHL, Optical Interference.

1. INTRODUCTION

Intermittent motion is one of the most common forms of movement in machineries, often found in chain drives, bearings, etc. This special motion pattern easily alters the lubrication state, leading to excessive wear and, in severe cases, potential reliability issues. The motion is a periodic one that repeats constant speed-deceleration-stop-acceleration- constant speed. For this special motion, Sperka *et al*. [1] explored the film thickness and pressure distributions in point contact based on experiments and theory. Sugimura *et al*. [2] studied EHL films under various unsteady motions, including acceleration/deceleration, stop/start, and reciprocating motion. Nishikawa *et al*. [3] investigated oil film variations in simple sliding reciprocating motion using optical interference technology and compared the results with those under unidirectional conditions. Venner *et al*. [4] simulated the effect of oscillatory entraining speed on film thickness in piezo-viscous regime on the calculation of film thickness under rapid time-varying conditions. Wang *et al*. [5] studied the thermal EHL problem of line contact under reciprocating motion and revealed the influence of working conditions such as frequency and load on film thickness, pressure, and traction coefficient during a cycle through numerical simulation. Zhao *et al*. [6] demonstrated that during deceleration, the pressure and film thickness distributions depend only on the instantaneous speed and not on the initial steady-state speed. Wang *et al*. [7] experimentally studied the effects of oil supply and entrainment speed on the oil film under intermittent motion. Wu *et al*. [8] demonstrated the effects of deceleration, stop time, and other working conditions on oil film characteristics under single and bidirectional intermittent motion conditions. Yao *et al*. [9] revealed the changes in the oil film in simple sliding intermittent motion by considering thermal effect. Similarly, Zhang *et al*. [10] studied numerically mixed thermal EHL by considering the existence of surface roughness in simple sliding intermittent motion and pointed out that in mixed lubrication state, the variation of the oil characteristics is quite different from those in smooth contact. Cen and Lugt *et al*. [11] revealed the differences in oil film changes during start and stop periods under different lubrication conditions. Sander and Allmaier *et al*. [12] studied the wear behavior in the contact area during start-stop processes. Zhang *et al*. [13] experimentally investigated the impact of intermittent motion cycles on film thickness and wear in the contact area, and employed acoustic emission (AE) signals to study the variation of surface wear.

Common oil film measurement methods mainly include capacitance method [14], ultrasonic measurement method [15], and relative optical intensity measurement method [16]. Compared to acoustic and electrical measurements, optical interferometric measurement method is less affected by external interference and can ensure measurement precision. Spikes *et al*. [17] proposed a method with better precision than traditional optical interferometry, which involved spraying a buffer layer on a chrome-plated

*Address correspondence to this author at the College of Mechanical Engineering, Donghua University, Shanghai, China;
E-mail: jingwang@dhu.edu.cn

E-ISSN: 2409-9848/24

glass disc. This method can accurately measure film thicknesses even below 10 nm. Johnston *et al*. [18] combined solid spacer layers with spectral analysis of reflected light at contact points, making optical interferometry applicable to some rolling contacts and extremely thin oil film thickness circumstances. Guo and Wong *et al*. [19] proposed a multi-beam intensity measurement technique (MBI) in 2002, which has been validated for film thickness within 1 nm. Liu *et al*. [20] have extended the range of film thickness measurements using red-green dual-color light, by subtracting the interference fringes produced by the dual-color light source to obtain the light intensity of the modulation signal relative to the film thickness. This greatly increased the measurement range to 10nm~4μm. It is also the film thickness measurement method used in this paper, namely the dichromatic interference intensity modulation (DIIM) technique.

2. EXPERIMENTAL EQUIPMENT AND CONDITIONS

2.1. Experimental Equipment and Principle

The experiments were conducted using a self-made ball-disk test rig, mainly composed of a motion control device, an image acquisition device, and a loading device. The schematic structure is shown in Figure **1**. The glass disk rotation was controlled by PLC programming to achieve intermittent motion. The speed variation within one intermittent motion cycle is shown in Figure **2**, which sequentially undergoes constant speed-deceleration-stop-acceleration periodic motion, while the pin remains fixed.

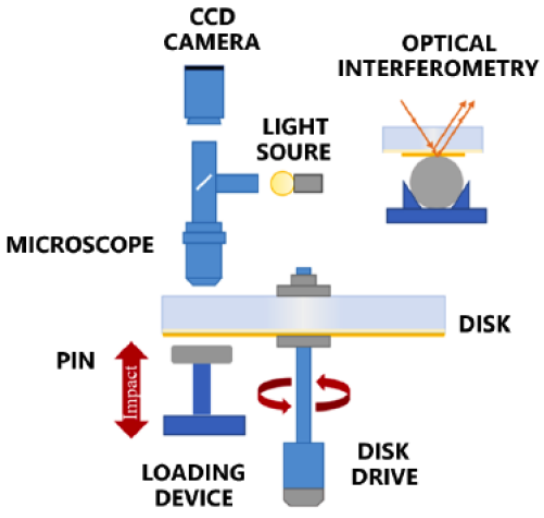

Figure 1: Schematic diagram of pin-disk test rig.

The image acquisition device mainly consists of a light source, a microscope, and a CCD industrial camera. The light source uses a red and green dual-color laser source (red wavelength λ = 653nm, green wavelength λ = 532nm), which are combined into a single beam directed at the pin-glass disk line contact area, generating red-green alternating optical interference fringes. The CCD camera captures the optical interference images magnified by the microscope, with a capture rate of 350 frames per second.

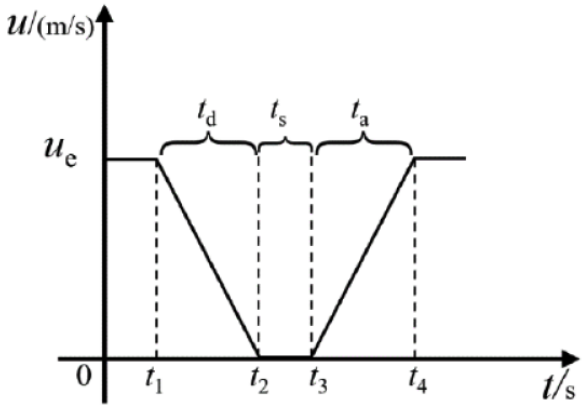

Figure 2: Variation of entraining speed.

2.2. Experimental Materials and Parameters

The material of the glass disk is K9 glass, with a diameter and thickness of 150 mm and 15 mm, respectively. The contact surface with the pin is coated with a 15nm nominal thickness reflective Chromium film and a 120 nm nominal thickness SiO_2 as buffer layer, with a surface roughness of 4 nm. The pin is a cylinder made of GCr15 steel, with a length of 13 mm, a radius of 6 mm. The specific parameters of the glass disk and the steel pin are shown in Table **1**. The specific parameters of the lubricating oil used in the experiment are shown in Table **2**.

After the experiment, the collected oil film interferograms were processed using the DIIM software [20]. This technique has a film thickness resolution of 1nm and can accurately measure the thickness of the lubricating oil film within a range of 0 ~ 4 μm.

During the experiments, the humidity was controlled at 40 ± 5% and the ambient temperature at 24 ± 0.5 ^{o}C. The pin remained fixed while the glass disk underwent intermittent motion. Oil was evenly and sufficiently applied to the contact surfaces of the glass disk and the pin, ensuring adequate oil supply.

Table 1: Parameters of the Pin and Disk

Performances	Pin	Disk
Material	GCr15 steel	K9 glass
Radius(mm)	6	75
Thickness(mm)	\	15
Length(mm)	13	\
Effective Young's modulus E'/GPa	210	81
Poisson's ratio μ	0.3	0.208
Density ρ/(kg/m^3)	7850	2510
Thermal conductivity k/(W·m^{-1}·K^{-1})	46	1.11
Specific heat c/(J·kg^{-1}·K^{-1})	470	840

Table 2: Parameters of PAO40 Oil

Properties	Value
Base oil viscosity (40°C mm^2/s)	496
Base oil viscosity (100 °C mm^2/s)	47
Density ρ/(kg/m^3)	850

3. RESULTS AND DISCUSSION

Figure **3** shows the oil film interferograms in the middle of the contact area at three different entraining speeds within one cycle. From left to right, the maximum entraining speeds are 0.8 m/s, 0.5 m/s, and 0.2 m/s, respectively. Additionally, a constant load of 100N was applied; the period of one intermittent motion cycle was 2.8 s, with a constant speed time of 0.5 s, a stop time of t_s = 0.8 s, and acceleration and deceleration times of t_a = t_d = 0.5 s and then a constant speed time of 0.5 s. The first image was scaled in two directions. A cross-section is chosen to measure the film thickness, as indicated by the dashed arrow in the first row. The corresponding cross-sectional film thickness curves along the *x*-direction are shown in Figure **4**.

Figure **3**(**a**) shows that during constant speed motion, the film thickness in the contact area remains stable. At an entraining speed of 0.2m/s, the oil film exhibits noticeable constriction at the exit. With the other two speeds, the oil film primarily exhibits a wedge shape with no obvious elastic deformation (Figure **4**(**a**)). Then, during the deceleration phase, as the speed decreases, the film thickness gradually reduces, and elastic deformation becomes noticeable and the exit constriction becomes more pronounced, as shown in Figures **4**(**b**)(**c**). When the speed is 0, with further enhancement of the squeeze effect, the center of the cross-sectional oil film curves at all three speeds exhibits an upward entrapment, indicating that some oil is entrapped at the center of the contact area(Figure (**d**)). Figure **3**(**e**) shows the beginning of the acceleration phase during the intermittent motion. As the speed increases, the oil entrapped in the center of the contact area is removed from the contact, and the lower film thickness oil formed at the entrance of the contact area moves towards the outlet area, passing through the contact area center, as shown in Figures **3**(**e**)~(**h**) and **4**(**e**)~(**h**). As the speed increases, the oil film thickness also gradually rises, and when the speed reaches its maximum, the oil film shape returns to a shape identical to the initial shape, as shown in Figure **3**(**k**) and **4**(**k**).

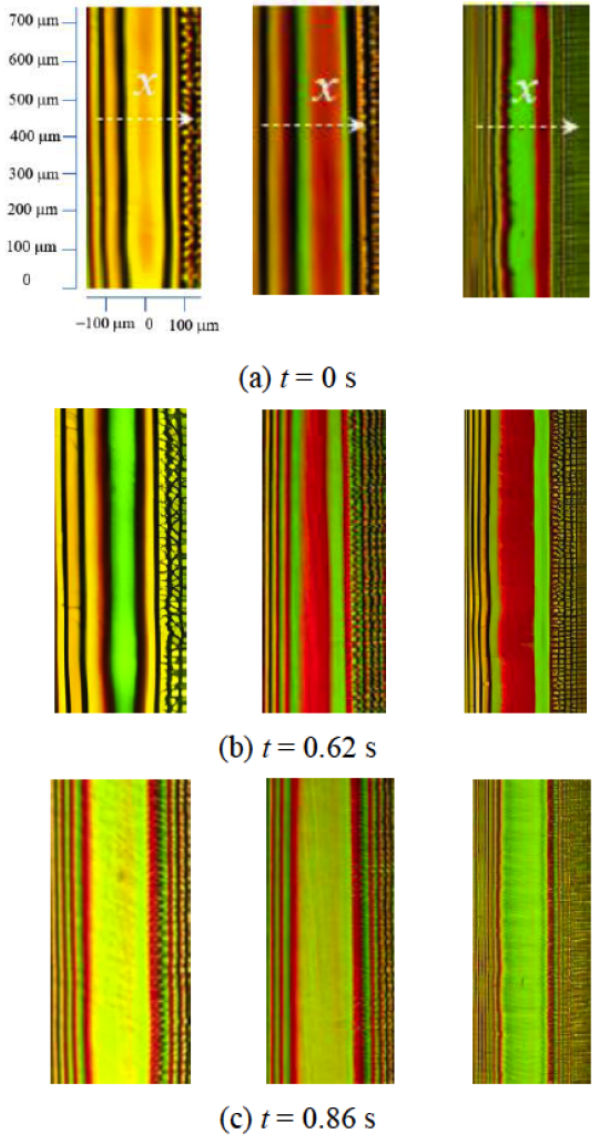

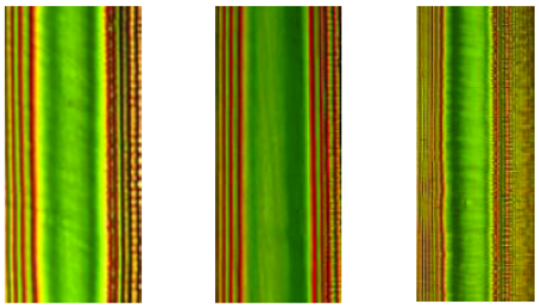

(d) $t = 1.0$ s

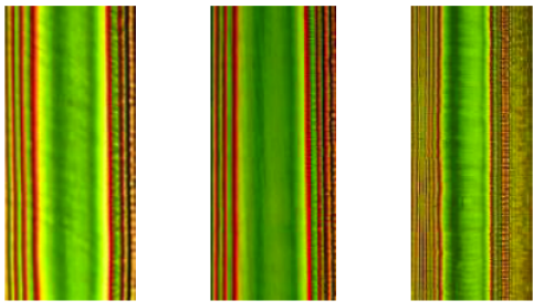

(e) $t = 1.85$ s

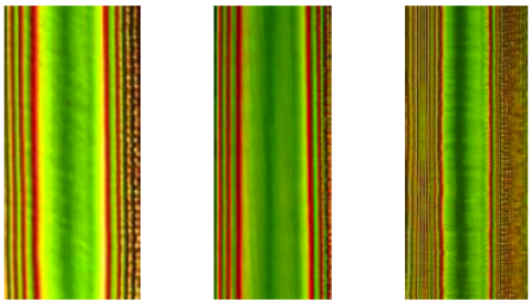

(f) $t = 1.92$ s

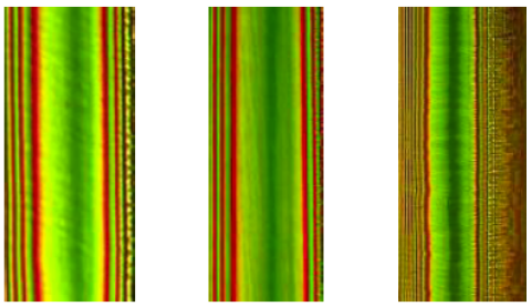

(g) $t = 1.96$ s

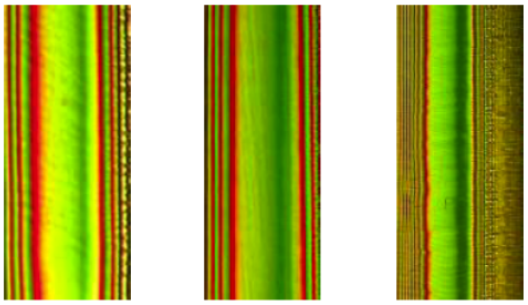

(h) $t = 2.02$ s

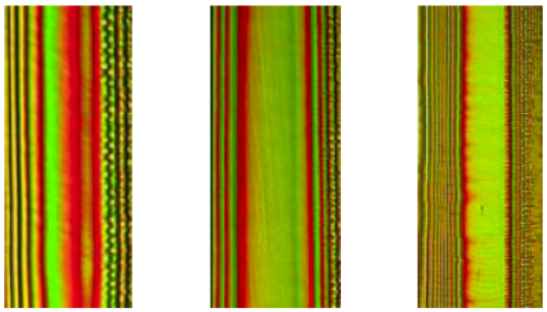

(i) $t = 2.09$ s

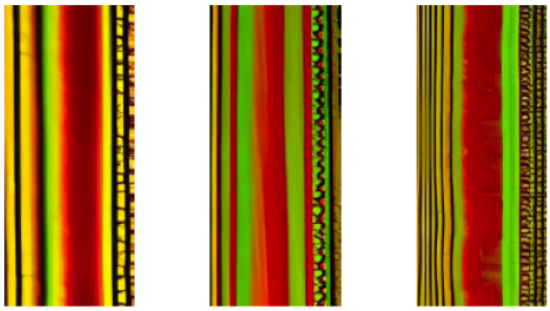

(j) $t = 2.2$ s

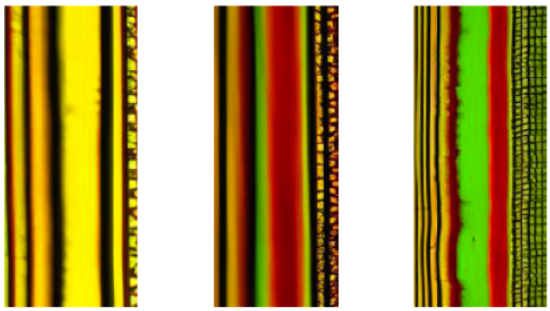

(k) $t = 2.8$ s

Figure 3: Optical interference images (w_{max} = 100 N).

Figure **5** shows the variations of central and minimum film thicknesses over one intermittent motion cycle for the three entraining speed conditions. The results indicate that film thickness is significantly influenced by speed. When the speed is non-zero, film thickness increases with the increase of the entraining speed. At the stop phase, the differences become not obvious. It can also be observed that at the beginning of the acceleration phase, there is a sudden drop in the central film thickness due to the newly formed oil film in the inlet region which passed through the contact afterwards.

Figure **6** shows the oil film interferogram at the end part of the pin within one cycle, with the cross-sectional oil film profile along the *x*-direction shown in Figure **7**, with an entraining speed of 0.5m/s. Compared to the optical interference images at the middle region, the

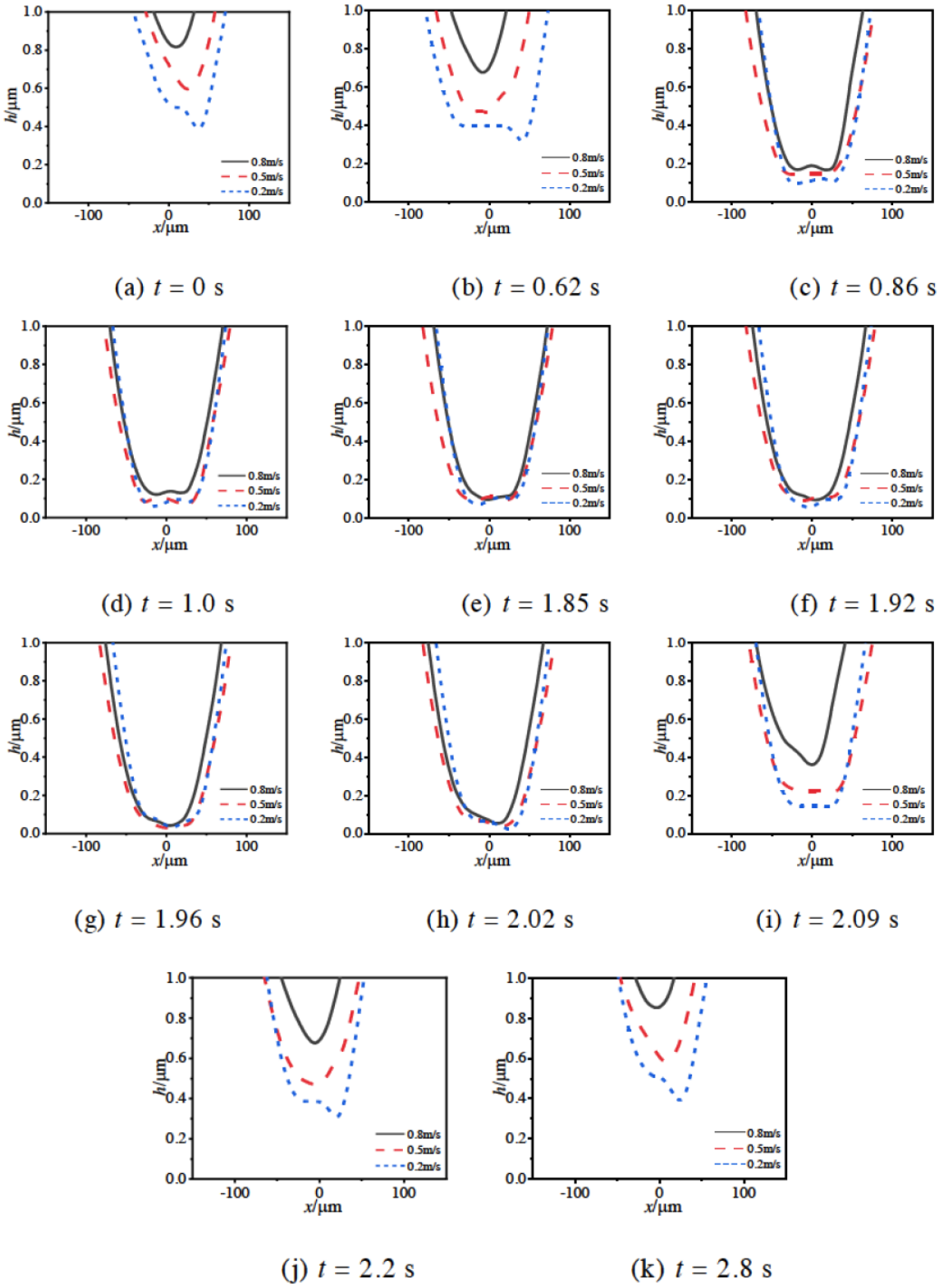

Figure 4: Cross-sectional Oil film curves along the *x*-direction(w_{max} = 100N).

constriction at end part of the contact area is more pronounced, with ear lobes appearing at both ends with the interior contact area appearing as a plain. The oil film thickness in Figure **8** is generally lower than the counterpart in Figure **5** and oil film shape during the entire intermittent motion stage looks different although the tendency is the same.

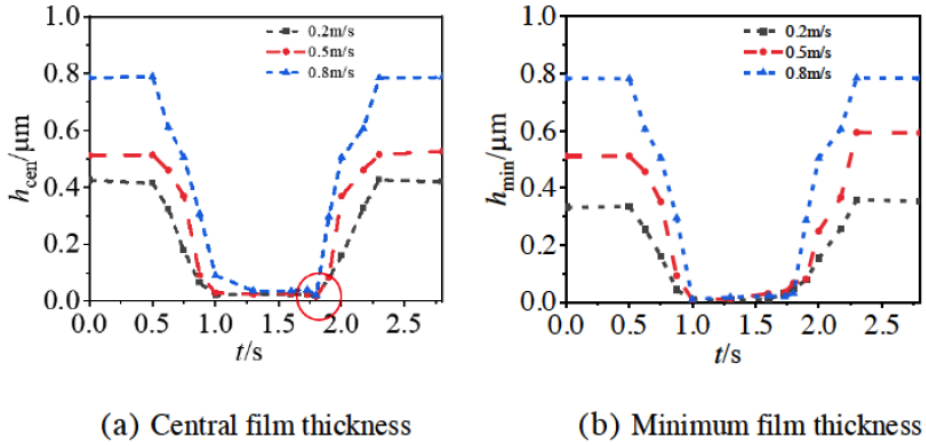

Figure 5: Central and minimum film thickness under three speed conditions(w_{max} = 100N).

Figure **8** shows the variation of central film thickness and minimum film thickness under three different loads, namely 40 N, 70 N, and 100 N, with an entraining speed of 0.5 m/s. Compared to the effect of entraining speed, the effect of load variation on film thickness is not that obvious. The greater the load, the smaller the central film thickness and the minimum film thickness. When the entraining speed is 0 at the stop phase, the influence of load on both central and minimum film thickness is slight.

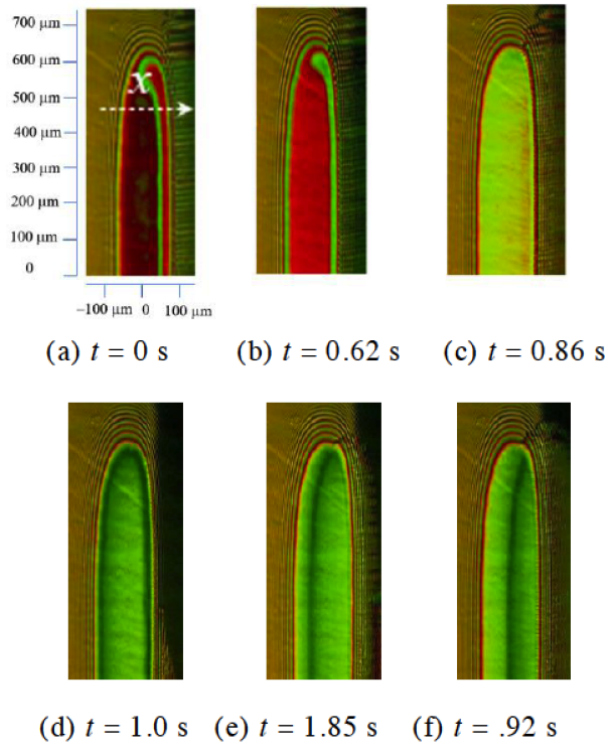

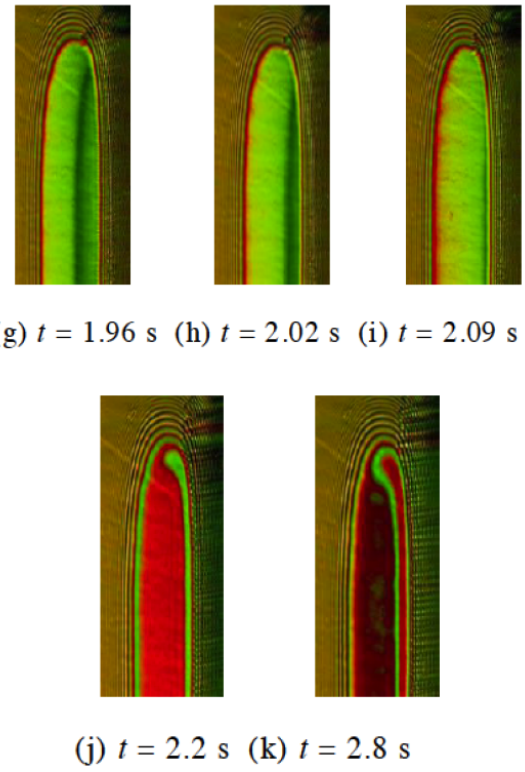

Figure 6: Optical interference images of oil film at the end of the pin (v = 0.5m/s,w_{max} = 100N).

Figure **9** shows the curves of central and minimum film thicknesses with different acceleration and deceleration times, specifically t_d = t_a = 0.2 s, 0.5 s, and 1.0 s, with a maximum speed of 0.5 m/s. A longer deceleration time indicates a smaller deceleration rate, thereby affecting the film thickness. From Figure **9**, it can be seen that the impact of acceleration and deceleration times on film thickness mainly occurs during the stop phase. Longer acceleration and

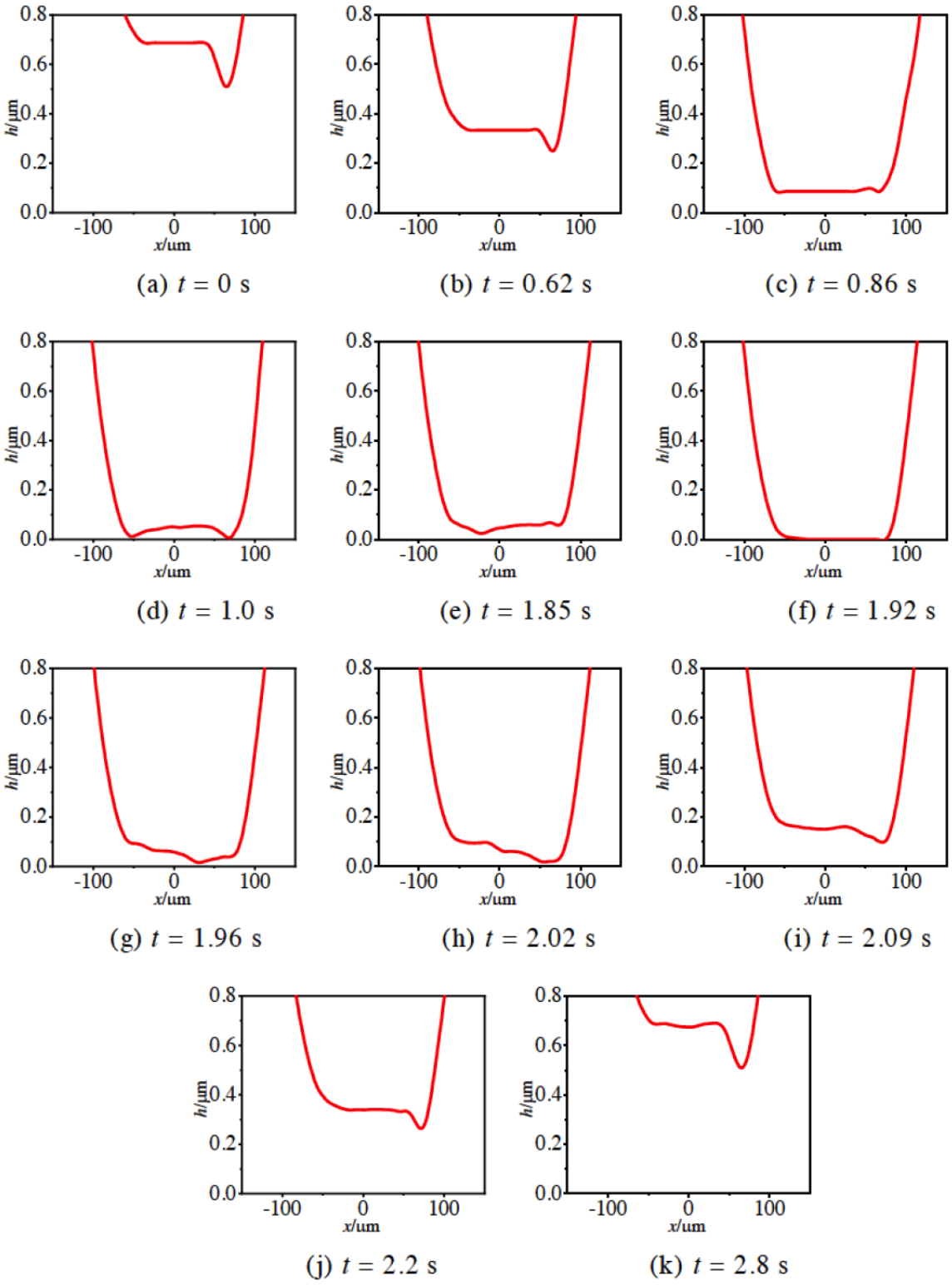

Figure 7: Cross-sectional oil film profiles along the *x*-direction at the end of the pin. (v = 0.5 m/s,w_{max} = 100 N)

deceleration times result in smaller acceleration and deceleration rates, leading to smaller central and minimum film thickness during the stop phase.

4.CONCLUSIONS

Using on the ball-disk optical interferometric test rig, the authors explored the oil film variation under

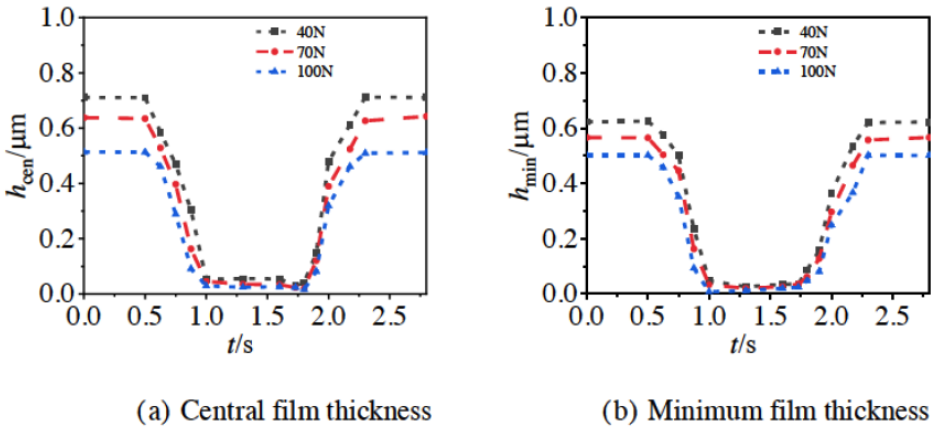

Figure 8: Central and minimum film thickness at different loads (v = 0.5 m/s).

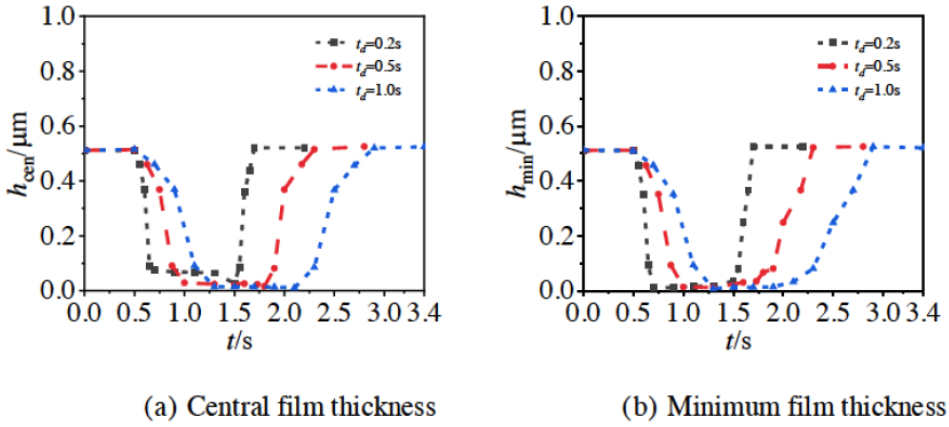

Figure 9: Central and minimum film thickness at different acceleration and deceleration times (v = 0.5 m/s, w_{max} = 100 N).

intermittent motion conditions from an experimental perspective and studied the effects of different maximum velocities, loads, and acceleration-deceleration times on the oil film.

(1) When the entraining speed increases, the oil film thickness also increases, and the film shape mainly takes a wedge-shape. At lower speeds, significant constriction can be observed at the outlet.

(2) Load and acceleration/deceleration times significantly impact the central film thickness; higher loads result in lower central film thickness. Shorter deceleration time, meaning higher deceleration rates, also lead to greater central film thickness. The effects of load and acceleration/deceleration times on the minimum film thickness are relatively minor.

CONFLICTS OF INTEREST

The authors declared no potential conflicts of interest with respect to the research, authorship, and/or publication of this article.

REFERENCES

[1] Sperka P, Wang J, Krupka I, *et al*. Occurrence of High Pressure Spike in Unidirectional Start-Stop-Start Point Contacts [J]. Journal of Tribology, 2014, 136(4): 041503. https://doi.org/10.1115/1.4028029

[2] Sugimura J, Jones Jr W, Spikes H. EHD film thickness in non-steady state contacts [J]. Journal of Tribology, 1998, 120(3): 442-452. https://doi.org/10.1115/1.2834569

[3] Nishikawa H, Handa K, Kaneta M. Behavior of EHL Films in Reciprocating Motion [J]. JSME international journal Ser C, Dynamics, control, robotics, design and manufacturing, 1995, 38(3): 558-567. https://doi.org/10.1299/jsmec1993.38.558

[4] Venner C H, Hagmeijer R. Film Thickness Variations in Elasto-Hydrodynamically Lubricated Circular Contacts Induced by Oscillatory Entrainment Speed Conditions [J]. Proceedings of the Institution of Mechanical Engineers, Part J: Journal of Engineering Tribology, 2008, 222(4): 533-547. https://doi.org/10.1243/13506501JET306

[5] Wang J, Kaneta M, Yang P. Numerical Analysis of TEHL Line Contact Problem under Reciprocating Motion [J]. Tribology International, 2005, 38(2): 165-178. https://doi.org/10.1016/j.triboint.2004.07.025

[6] Zhao J, Sadeghi F. Analysis of EHL Circular Contact Shut Down [J]. J Trib, 2003, 125(1): 76-90. https://doi.org/10.1115/1.1481366

[7] Wang F, Study on the EHL Oil Films under Intermittent Motion[D], Qingdao University of Technology, China, 2014.

[8] Wu D, Wang J, Kaneta, M, Performance of EHL Oil Film in Intermittent Motion, Tribology Online, 2018, 13(4): 204-211. https://doi.org/10.2474/trol.13.204

[9] Yao M L, Numerical Analysis of Thermal EHL of Roller Chains under Intermittent Motion[D], Donghua University, China, 2021.

[10] Zhang M Y, Yao M L, Wang J, *et al*. Point Contact Thermal Mixed Elastohydrodynamic Lubrication under Short-Period Intermittent Motion [J]. Journal of Tribology, 2023, 145(8): 082202. https://doi.org/10.1115/1.4062098

[11] Cen H, Lugt P M. Effect of Start-Stop Motion on Contact Replenishment in A Grease Lubricated Deep Groove Ball Bearing [J]. Tribology International, 2021, 157: 106882. https://doi.org/10.1016/j.triboint.2021.106882

[12] Sander D E, Allmaier H. Starting and Stopping Behavior of Worn Journal Bearings [J]. Tribology International, 2018, 127: 478-488. https://doi.org/10.1016/j.triboint.2018.06.031

[13] Zhang M Y, Wang X Q, Han Y M, *et al*. Point Contact EHL and Wear in Intermittent Motion [J]. Journal of Tribology, 2024: 1-32.

[14] Zhang P S, Zhu B, Liu S, *et al*. Study of Measuring EHL Oil-Film Thickness with Electric Capacity Method [J]. Lubrication Engineering, 1982, (02): 18-24.

[15] Dwyer-Joyce R S, Reddyhoff T, Drinkwater B. Operating Limits for Acoustic Measurement of Rolling Bearing Oil Film Thickness [J]. Tribology Transactions, 2004, 47(3): 366-375. https://doi.org/10.1080/05698190490455410

[16] Huang P, Luo J B, *et al*. Investigation into Measuring Nanometer Lubrication Film Thickness by Relative Light Intensity Principle [J]. Lubrication Engineering, 1995, (01): 32-34. (In Chinese)

[17] Spikes H, Guangteng G. Paper Xi (I) Properties of Ultra-Thin Lubricating Films Using Wedged Spacer Layer Optical Interferometry[M]. Tribology Series. Elsevier. 1987: 275-279. https://doi.org/10.1016/S0167-8922(08)71076-9

[18] Johnston G, Wayte R, Spikes H. The Measurement and Study of Very Thin Lubricant Films in Concentrated Contacts [J]. Tribology Transactions, 1991, 34(2): 187-194. https://doi.org/10.1080/10402009108982026

[19] Guo F, Wong P. A Multi-Beam Intensity-Based Approach for Lubricant Film Measurements in Non-Conformal Contacts [J]. Proceedings of the Institution of Mechanical Engineers, Part J: Journal of Engineering Tribology, 2002, 216(5): 281-291. https://doi.org/10.1243/135065002760364822

[20] Liu H C, Guo F, Guo L, *et al*. A Dichromatic Interference Intensity Modulation Approach to Measurement of Lubricating Film Thickness [J]. Tribology Letters, 2015, 58: 1-11. https://doi.org/10.1007/s11249-015-0480-y

Received on 23-07-2024 Accepted on 28-08-2024 Published on 19-09-2024

https://doi.org/10.31875/2409-9848.2024.11.03